Mon. Not. R. Astron. Soc. **000**, 1–9 (2016) Printed 15 April 2016 (MN LATEX style file v2.2)

Chemistry and Kinematics of Red Supergiant Stars in the Young Massive Cluster NGC 2100

L. R. Patrick[1⋆], C. J. Evans[1,2], B. Davies[3], R-P. Kudritzki[4,5], V. Hénault-Brunet[6], N. Bastian[3], E. Lapenna[7,8], M. Bergemann[9],

[1] *Institute for Astronomy, University of Edinburgh, Royal Observatory Edinburgh, Blackford Hill, Edinburgh EH9 3HJ, UK*
[2] *UK Astronomy Technology Centre, Royal Observatory Edinburgh, Blackford Hill, Edinburgh EH9 3HJ, UK*
[3] *Astrophysics Research Institute, Liverpool John Moores University, Liverpool Science Park ic2, 146 Brownlow Hill, Liverpool L3 5RF, UK*
[4] *Institute for Astronomy, University of Hawaii, 2680 Woodlawn Drive, Honolulu, HI, 96822, USA*
[5] *University Observatory Munich, Scheinerstr. 1, D-81679, Munich, Germany*
[6] *Department of Physics, Faculty of Engineering and Physical Sciences, University of Surrey, Guildford, GU2 7XH, UK*
[7] *Dipartimento di Fisica e Astronomia, Universitá degli Studi di Bologna, Viale Berti Pichat 6/2, I-40127 Bologna, Italy*
[8] *INAF-Osservatorio Astronomico di Bologna, via Ranzani 1, I-40127, Bologna, Italy*
[9] *Max-Planck Institute for Astronomy, D-69117, Heidelberg, Germany*

arXiv:1602.02702v2 [astro-ph.SR] 14 Apr 2016

Accepted Received 1; in original form

ABSTRACT

We have obtained *K*-band Multi-Object Spectrograph (KMOS) near-IR spectroscopy for 14 red supergiant stars (RSGs) in the young massive star cluster NGC 2100 in the Large Magellanic Cloud (LMC). Stellar parameters including metallicity are estimated using the *J*-band analysis technique, which has been rigorously tested in the Local Universe. We find an average metallicity for NGC 2100 of $[\mathrm{Z}] = -0.43 \pm 0.10$ dex, in good agreement with estimates from the literature for the LMC. Comparing our results in NGC 2100 with those for a Galactic cluster (at Solar-like metallicity) with a similar mass and age we find no significant difference in the location of RSGs in the Hertzsprung–Russell diagram. We combine the observed KMOS spectra to form a simulated integrated-light cluster spectrum and show that, by analysing this spectrum as a single RSG, the results are consistent with the average properties of the cluster. Radial velocities are estimated for the targets and the dynamical properties are estimated for the first time within this cluster. The data are consistent with a flat velocity dispersion profile, and with an upper limit of 3.9 km s^{-1}, at the 95% confidence level, for the velocity dispersion of the cluster. However, the intrinsic velocity dispersion is unresolved and could, therefore, be significantly smaller than the upper limit reported here. An upper limit on the dynamical mass of the cluster is derived as $M_{dyn} \leqslant 15.2 \times 10^4 M_{\odot}$ assuming virial equilibrium.

Key words: stars: abundance, (stars:) supergiants, (galaxies:) Magellanic Clouds, galaxies: star clusters: individual: NGC 2100

1 INTRODUCTION

Young massive clusters (YMCs[1]) are important probes of the early evolution of star clusters and have increasingly been used as tracers of star formation in galaxies (e.g. Whitmore & Schweizer 1995; Miller et al. 1997; Zepf et al. 1999). Known to contain large populations of massive stars, YMCs are also important tracers of massive star formation, which is heavily clustered (Lada & Lada 2003; de Wit et al. 2005; Parker & Goodwin 2007). In addition to being the birthplace of most of the massive stars in the Local Universe ($> 200\,\mathrm{M}_{\odot}$ stars in R136; Crowther et al. 2010), owing to the density of stars, YMCs are thought to be the birthplace of some of the rich stellar exotica (e.g. blue stragglers, X-ray binaries and radio pulsars) found in the old population of globular clusters (GCs; Portegies Zwart et al. 2010).

Recently, the idea that GCs are simple stellar populations has been called into question based on chemical anomalies of light elements (C, N, O, Na and Al; e.g. Gratton et

⋆ E-mail: lrp@roe.ac.uk

[1] A YMC is defined as having an age of < 100 Myr and a stellar mass of $> 10^4\,\mathrm{M}_{\odot}$ (Portegies Zwart et al. 2010).

© 2016 RAS

al. 2012). These anomalies are considered by most authors to be the signature of multiple stellar populations within GCs. Studying YMCs could therefore potentially help to constrain some of the proposed models for creating multiple stellar populations within GCs (e.g. Cabrera-Ziri et al. 2014).

Investigating the link between YMCs and older clusters is an important, uncertain, factor in the evolution of young clusters. As most stellar systems are thought to dissolve shortly after formation (Lada & Lada 2003), determining how long bound systems can remain so is an important question to answer. Studying the dynamical properties of YMCs is, therefore, an important tool to evaluate the likelihood that young clusters will survive. In addition, the study of YMCs in different environments can help bridge the gap between the understanding of star formation in the Solar neighbourhood and that in the high-redshift Universe.

Over the last few years, medium resolution ($R \geqslant 3000$) near-IR spectroscopy has been shown to be a powerful tool to estimate stellar parameters for red supergiant stars (RSGs; Davies et al. 2010). RSGs are the final evolutionary stage of a massive star and, owing to their cool atmospheres ($T_{\rm eff} \sim 4000$ K; Davies, B., et al. 2013), are brightest at $\sim 1.1\,\mu$m. In star-forming galaxies, RSGs are the most luminous near-IR sources, therefore, they can be observed out to large distances at these wavelengths. Given that dust extinction is intrinsically lower at near-IR wavelengths and that the next generation of ground-/space-based telescopes will be optimised for observations at these wavelengths, RSGs are likely to become increasingly attractive targets by which to study distant star-forming galaxies.

The J-band analysis technique for estimating metallicities and stellar parameters of RSGs has been rigorously tested by Gazak et al. (2014a) and Davies et al. (2015). These authors show that metallicities can be estimated in extragalactic systems to a high level of accuracy and to a precision of < 0.15 dex.

The availability of the K-band multi-object spectrograph (KMOS; Sharples et al. 2013) at the Very Large Telescope (VLT), has presented new opportunities for efficient observations of samples of RSGs in external galaxies to study their distribution and build-up of metals. Patrick et al. (2015) used KMOS observations to investigate the present-day metallicity of NGC 6822 ($d = 0.5$ Mpc) and Gazak et al. (2015) determined the metallicity gradient of NGC 300, a grand design spiral galaxy outside the Local Group ($d = 1.9$ Mpc), finding striking agreement with previous measurements from stars and H II regions.

In addition, Gazak et al. (2013) demonstrated that, after the appearance of the first RSGs within a YMC, the overall near-IR flux from the cluster is dominated by the RSGs ($F_{J,RSG}/F_J > 0.90$). Using this result, these authors showed that the spectrum from an unresolved star cluster can be used to estimate the average properties of the RSG population of the cluster using exactly the same analysis method as for single stars. Lardo et al. (2015) demonstrated this with KMOS spectroscopy of three unresolved YMCs in NGC 4038 in the Antennae ($d = 20$ Mpc), at Solar-like metallicity, finding good agreement with previous studies. With a multi-object spectrograph operating on the European Extremely Large Telescope, this technique could be used to measure metallicities of individual RSGs at distances of > 10 Mpc and from YMCs out to potentially > 100 Mpc (Evans et al. 2011).

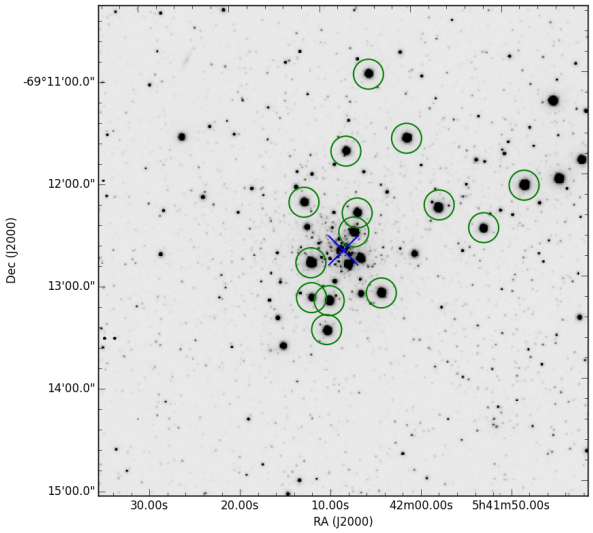

Figure 1. Positions of the KMOS targets in NGC 2100 overlaid on a VISTA J-band image (Cioni et al. 2011). Green circles indicate KMOS targets. The adopted cluster centre has been marked by a blue cross.

NGC 2100 is a YMC in the Large Magellanic Cloud (LMC), located near the large star-forming 30 Doradus region. With an age of ~ 20 Myr (Elson 1991; Niederhofer et al. 2015), and a photometric mass of $4.6 \times 10^4 M_\odot$ (McLaughlin & van der Marel 2005, assuming King (1966) profiles), NGC 2100 falls within the mass and age range where the near-IR cluster light is dominated by RSGs (Gazak et al. 2013). This is supported by the large number of RSGs identified within this cluster (see Figure 1).

NGC 2100 is not a cluster in isolation. It is located in one of the most actively star-forming regions within the Local Group of galaxies. At ~ 20 Myr old, the most massive members of this star cluster will have already exploded as supernovae. This should have had a profound effect on the surrounding gas and dust, and has potentially shaped the surrounding LMC 2 supershell (see Points et al. 1999).

In this study we estimate stellar parameters from KMOS spectroscopy for 14 RSGs which appear to be associated with NGC 2100. Section 2 describes the observations and data reduction, and in Section 3 we detail our results, focusing on radial velocities of the target stars where we derive the line-of-sight velocity dispersion, the dynamical mass of NGC 2100 and stellar parameters. Our results are discussed in Section 4 and conclusions are presented in Section 5.

2 OBSERVATIONS AND DATA REDUCTION

These observations were obtained as part of the KMOS Guaranteed Time Observations (PI: Evans 095.B-0022) in March 2015. The observations consisted of 8×10 s exposures (seeing conditions $\sim 1\farcs0$) taken with the YJ grating with sky offset exposures (S) interleaved between the object

exposures (O) in an O, S, O observing pattern. In addition, a standard set of KMOS calibration frames were obtained as well as observations of HD 51506 (B5) as the telluric standard star. Figure 1 shows the observed RSGs overlaid on a *J*-band VISTA image of the surrounding region (Cioni et al. 2011).

The standard KMOS/esorex routines (SPARK; Davies, R. I., et al. 2013) were used to calibrate and reconstruct the data cubes. Telluric correction was performed using observations of the standard star in all 24 IFUs using the methodology described in detail by Patrick et al. (2015). Briefly, corrections are made to the standard telluric recipe to account for slight differences in wavelength calibration between the telluric and science spectra. This is implemented using an iterative cross-correlation approach. Additionally, differences in the strength of the telluric features are corrected by applying a simple scaling using the equation:

$$T_2 = (T_1 + c)/(1 + c) \quad (1)$$

where T_2 is the scaled telluric-standard spectrum, T_1 is the uncorrected telluric-standard spectrum and c is the scaling parameter which is varied from $c = -0.5$ to $c = 0.5$ in increments of 0.02. The best value of c is chosen based on the overall standard deviation of the spectrum, i.e. the c value producing the smallest σ is selected. Once these corrections are accounted for, the science spectra are divided by the appropriate telluric spectrum for that particular KMOS integral field unit (IFU).

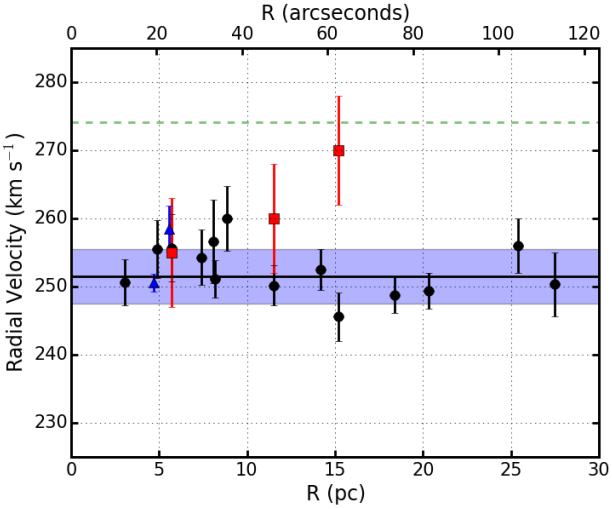

Figure 2. Radial velocities of KMOS targets (black points) shown as a function of distance from the cluster centre. The green dashed line shows the LMC systemic velocity of ∼200 massive stars from (274.1 ± 16.4 km s^{-1}; Evans et al. 2015). The solid black line shows the mean cluster velocity ($v_0 = 251.6 \pm 1.1$ km s^{-1}) and the shaded blue region shows $v_0 \pm \sigma_{1D}$. The blue triangles show estimates for two OB-type stars in NGC 2100 (Evans et al. 2015) and the red squares show previous estimates for three of our targets (Jasniewicz & Thevenin 1994). The distance modulus used to produce this figure is 18.5 (Pietrzyński et al. 2013; de Grijs et al. 2014).

3 RESULTS

3.1 Radial velocities and velocity dispersion

Radial velocities are estimated using an iterative cross-correlation method. To ensure systematic shifts are removed, the observed spectra are first cross-correlated against a spectrum of the Earth's atmosphere, taken from the European Southern Observatory web pages[2], at a much higher spectral resolution than that of KMOS. This spectrum is then degraded to the resolution of the observations using a simple Gaussian filter. The cross-correlation is performed within the 1.140–1.155 μm region, as a strong set of reliable telluric features dominates this region, with minimal contamination from stellar features. The shift arising from this comparison is typically 0–10 km s^{-1} and is then applied to the science spectra so that they are on a consistent wavelength solution.

Stellar radial velocities are estimated following a similar approach to the methods used by Lapenna et al. (2015) and Patrick et al. (2015). An initial radial-velocity estimate is found for each star from cross-correlation of the KMOS spectra with an appropriate model spectrum in the 1.16–1.22 μm region (selected owing to the dominance of atomic features in RSG spectra at these wavelengths). We improved on this initial estimate via independent cross-correlation of the observed and model spectra for seven strong absorption lines in this region.

The quoted radial velocity for each star is the mean of these estimates, where the quoted uncertainty is the standard error of the mean (i.e. $\sigma/\sqrt{n_{\rm lines}}$). Obvious outliers (with δRVs of tens of km s^{-1}) were excluded in calculating the mean estimates; such outliers arise occasionally from spurious peaks in the cross-correlation functions from noise/systematics in the spectra.

In order to sample from the posterior probability distribution for the intrinsic velocity dispersion and mean cluster velocity (given the observed radial velocity estimates and their uncertainties), we use `emcee` (Foreman-Mackey et al. 2013), an implementation of the affine-invariant ensemble sampler for Markov chain Monte Carlo (MCMC) of Goodman & Weare (2010). Our likelihood function is given by

$$p(D|\{\sigma_{1D}, v_0\}) = \prod_i \frac{1}{\sqrt{2\pi(\sigma_{1D}^2 + \sigma_{v,i}^2)}} \exp\left(\frac{-(v_i - v_0)^2}{2(\sigma_{1D}^2 + \sigma_{v,i}^2)}\right), \quad (2)$$

where σ_{1D} is the intrinsic velocity dispersion of the cluster, v_0 is the mean cluster velocity, and the data consists of our set of radial velocity measurements v_i and their uncertainties $\sigma_{v,i}$. We therefore assume that the intrinsic cluster dispersion is Gaussian with no variations in the dispersion across the sample. The systemic radial velocity (v_0) of the sample is estimated to be 251.6 ± 1.1 km s^{-1}.

Table 1 displays our stellar radial-velocity estimates and Figure 2 shows these estimates as a function of distance from the centre of the cluster, compared with the average radial velocity of ∼200 massive stars within the LMC from Evans et al. (2015, green dashed line). To quantify the likelihood that the measured velocities are consistent with the NGC 2100 mean cluster velocity we calculate the probability that each measured velocity is drawn from a two-component mixture of Gaussian distributions with

[2] Retrieved from http://www.eso.org/sci/facilities/paranal/decommissioned/isaac/tools/spectroscopic_standards.html

Table 1. Observed properties of VLT-KMOS targets in NGC 2100.

ID	S/N	J^{a}	H^{a}	$K_s{}^{a}$	RV (km s^{-1})	Notes[b]
J054147.86−691205.9	320	9.525	8.603	8.200	250.3 ± 4.7	D15
J054152.51−691230.8	200	10.413	9.526	9.155	249.3 ± 2.6	D16
J054157.44−691218.1	200	9.811	9.036	8.738	245.6 ± 3.5	C2
J054200.74−691137.0	260	9.900	9.017	8.683	248.8 ± 2.7	C8
J054203.90−691307.4	250	9.839	8.996	8.740	251.1 ± 2.8	B4
J054204.78−691058.8	210	10.319	9.427	9.159	256.1 ± 4.0	...
J054206.36−691220.2	200	10.371	9.480	9.159	255.7 ± 4.9	B17
J054206.77−691231.1	250	9.977	9.150	8.807	250.6 ± 3.4	A127
J054207.45−691143.8	200	10.482	9.610	9.351	252.5 ± 3.0	C12
J054209.66−691311.2	240	9.976	9.136	8.841	254.3 ± 4.1	B47
J054209.98−691328.8	250	10.021	9.150	8.823	250.2 ± 3.0	C32
J054211.56−691248.7	300	9.557	8.617	8.264	255.5 ± 4.3	B40
J054211.61−691309.2	150	10.943	10.090	9.788	256.6 ± 6.1	B46
J054212.20−691213.3	200	10.440	9.622	9.335	260.0 ± 4.8	B22

[a] Photometric data from 2MASS, with tyipcal errors on J, H, and K_s of 0.024, 0.026 and 0.022 mag respectively.
[b] Cross-identifications in final column from Robertson (1974).

$P(x|\{\mu,\sigma\}_{NGC\,2100}) + P(x|\{\mu,\sigma\}_{LMC-field}) = 1$, where the *LMC-field* distribution is defined by Evans et al. (2015).

From this analysis one target (J054212.20−691213.3) has a measured velocity with greater probability of being drawn from the underlying distribution of massive stars rather than the distribution centred on the NGC 2100 systemic velocity. Excluding this target from the sample does not alter the estimation of v_0 or σ_{1D} significantly, therefore we choose to include this target for further analysis.

We conclude that all targets have a velocity consistent with membership to the LMC (as opposed to Galactic objects) and that none display compelling evidence for being excluded from membership of NGC 2100.

The estimated v_0 is in reasonable agreement with previous measurements for two OB-type stars in the cluster (Evans et al. 2015) as well as the results from four RSGs in NGC 2100 (Jasniewicz & Thevenin 1994, henceforth JT94; three of which were observed in the current study). Table 2 contains the details of previous radial velocity measurements within NGC 2100. We conclude that there exists no significant difference between our measurements and previous estimates within NGC 2100. This is an additional confirmation that absolute radial velocities can be precisely measured with KMOS spectra.

As shown in Figure 3, the line-of-sight velocity dispersion (σ_{1D}) of NGC 2100 is unresolved given the current data. We can therefore place an upper limit on $\sigma_{1D} < 3.9\,\mathrm{km\ s^{-1}}$ at the 95% confidence level. In Figure 4 we demonstrate that we find no evidence for spatial variations in the measured σ_{1D} and we note that in each radial bin (which contain 5, 4 and 5 stars respectively), the measured dispersion is unresolved.

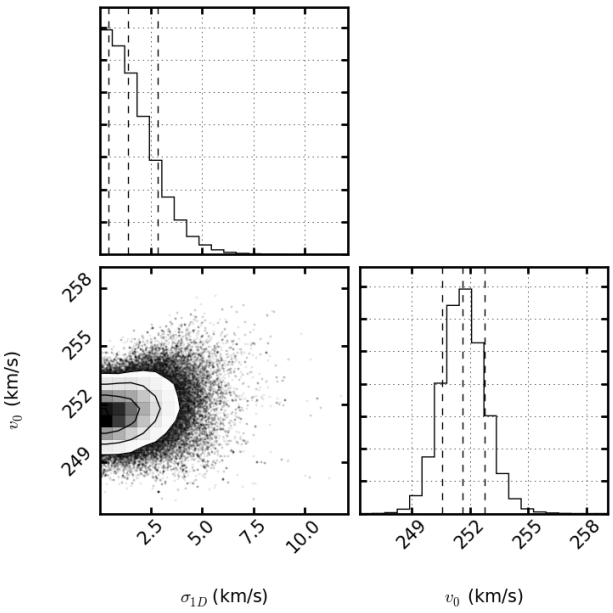

Figure 3. One- and two-dimensional projections of the posterior probability distributions of the line-of-sight velocity dispersion (σ_{1D}) and systemic velocity (v_0) for NGC 2100 assuming the dispersion is Gaussian and constant over the range measured. Using this method the velocity of NGC 2100 is $251.6 \pm 1.1\,\mathrm{km\ s^{-1}}$. This figure also demonstrates that the velocity dispersion for the sample is unresolved, we can therefore place an upper limit on $\sigma_{1D} < 3.9\,\mathrm{km\ s^{-1}}$ at the 95% confidence level. The vertical dashed lines in these figures indicate the estimated parameters with their associated $1\,\sigma$ uncertainties.

3.2 Dynamical mass

Using σ_{1D} as an upper limit on the velocity distribution, one can calculate an upper limit on dynamical mass of the cluster using the virial equation:

$$M_{dyn} = \frac{\eta \sigma_{1D}^2 r_{\mathrm{eff}}}{G} \tag{3}$$

where M_{dyn} is the dynamical mass and $\eta = 6 r_{vir}/r_{\mathrm{eff}} = 9.75$ – providing the density profile of the cluster is sufficiently steep (Portegies Zwart et al. 2010) – where $r_{\mathrm{eff}} = 4.41$ pc for NGC 2100 (McLaughlin & van der Marel 2005). However, NGC 2100 has a relatively shallow density profile ($\gamma = 2.44 \pm 0.14$; Mackey & Gilmore 2003) which means $\eta < 9.75$. Using $\sigma_{1D} = 3.9\,\mathrm{km\ s^{-1}}$ and equation 3, an upper limit on the dynamical mass of NGC 2100 is $M_{dyn} = 15.2 \times 10^4 M_\odot$. Comparing this to the photometric mass $M_{phot} = (2.3 \pm$

Table 2. Literature stellar radial-velocity measurements within NGC 2100.

ID		RV (km s^{-1})		Reference	Notes
Lit.	current study	Lit.	current study		
AAΩ 30 Dor 407	—	258.5 ± 3.4	...	Evans et al. (2015)	O9.5 II
AAΩ 30 Dor 408	—	250.6 ± 1.3	...	Evans et al. (2015)	B3 Ia
R74 B17	J054206.36-691220.2	255 ± 8	255.7 ± 4.9	Jasniewicz & Thevenin (1994)	
R74 C2	J054157.44-691218.1	270 ± 8	245.6 ± 3.5	Jasniewicz & Thevenin (1994)	
R74 C32	J054209.98-691328.8	260 ± 8	250.2 ± 3.0	Jasniewicz & Thevenin (1994)	
R74 C34	—	265 ± 8	...	Jasniewicz & Thevenin (1994)	

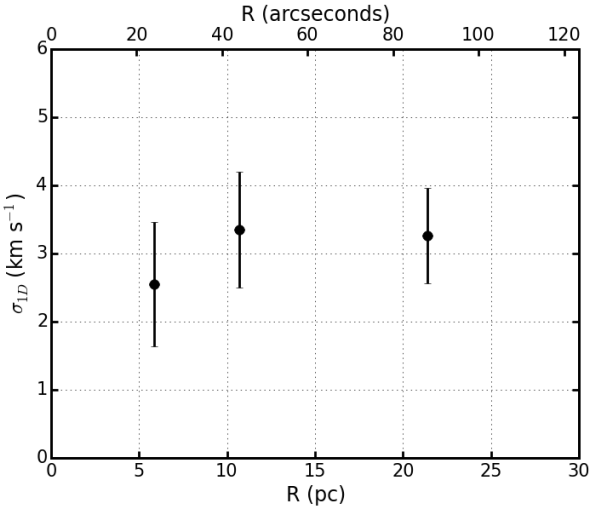

Figure 4. Upper limits to the line-of-sight velocity dispersion for the NGC 2100 RSGs in three radial bins as a function of the distance from the centre of NGC 2100. This figure demonstrates that we find no evidence for spatial variations in σ_{1D}. However, we note that in each radial bin the underlying dispersion is unresolved (see Figure 3).

$1.0) \times 10^4 M_\odot$ (McLaughlin & van der Marel 2005), we see that the upper limit on the dynamical mass is larger.

As discussed by Gieles et al. (2010), binary motions can increase the measured velocity dispersion profile (e.g. see Hénault-Brunet et al. 2012). However, as Gieles et al. (2010) note, the mean lifetime for RSGs in binary systems is significantly decreased and, where mass transfer occurs, their number decrease dramatically (Eldridge et al. 2008). We therefore expect that the number of RSGs in close binaries is small (Feast 1979; Davies et al. 2009). The fraction of RSGs in longer-period systems is less certain, but these would contribute substantially less to the line-of-sight velocity distribution.

These arguments suggest that our estimate for the velocity dispersion in NGC 2100 is not significantly increased by binary motions as our target stars are expected to be (predominantly) single objects. As the true dispersion of the cluster appears to be unresolved (Figure 3), we conclude therefore that the upper limit of the dynamical mass is consistent with the published photometric mass.

Evidence in the literature suggests that J054211.61−691309.2 is an eclipsing binary system VV Cep (Feast 1979). The radial velocity of this star (256.6 ± 6.1 km s^{-1}) appears to be slightly enhanced with respect to systemic velocity of NGC 2100, however, further study would be required to unambiguously classify this object as a binary.

3.3 Stellar parameters

Stellar parameters are estimated for each target using the J-band analysis technique described initially by Davies et al. (2010) and tested rigorously by Gazak et al. (2014a) and Davies et al. (2015). These studies show that by using a narrow spectral window within the J-band one can accurately derive overall metallicities ($[Z] = \log(Z/Z_\odot)$) to better than ± 0.15 dex at the resolution of KMOS observations with S/N $\geqslant$ 100. Patrick et al. (2015) built on this by demonstrating the feasibility of this technique using KMOS spectra.

The analysis uses synthetic RSG spectra, extracted from MARCS model atmospheres (Gustafsson et al. 2008), computed with corrections for non-local thermodynamic equilibrium for lines from titanium, iron, silicon and magnesium (Bergemann et al. 2012, 2013, 2015). The parameter ranges for the grid of synthetic RSG spectra are listed in Table 3. The synthetic spectra are compared with observations using the χ-squared statistic and the synthetic spectra are degraded to the resolution and sampling of the observations. The diagnostic spectral features used to estimate stellar parameters have equal weighting in the analysis.

Estimated stellar parameters are listed in Table 4. Figure 5 shows the observed KMOS spectra (black) compared to their best-fitting models (red). The average metallicity for the 14 RSGs is $[Z] = -0.38 \pm 0.20$ dex where the large scatter is a result of the contribution from (J054211.61−691309.2). Excluding this apparent outlier yields an average metallicity of $[Z] = -0.43 \pm 0.10$ dex, which reduces the scatter and does not alter the result significantly. The model fit parameters of J054211.61−691309.2 suggest a considerably ($\times 1.7$) super-solar metallicity. This appears unlikely given its apparent membership to the LMC, and it is notable that the estimates for the surface gravity and microturbulence parameters are also outliers compared to the rest of the sample. In addition, as noted above, this star was flagged as a potential eclipsing binary by (Feast 1979), therefore this target is excluded from the sample in further analysis.

The average metallicity in NGC 2100 estimated here is in good agreement with estimates of the cluster metallicity using isochrone fitting to the optical colour-magnitude diagram (−0.34 dex; Niederhofer et al. 2015). The only other estimate of stellar metallicity within this cluster is from JT94 who estimated metallicities using optical spectroscopy of four RSGs. These authors found an average metallicity for NGC 2100 of $[Fe/H] = -0.32 \pm 0.03$ dex, which is in rea-

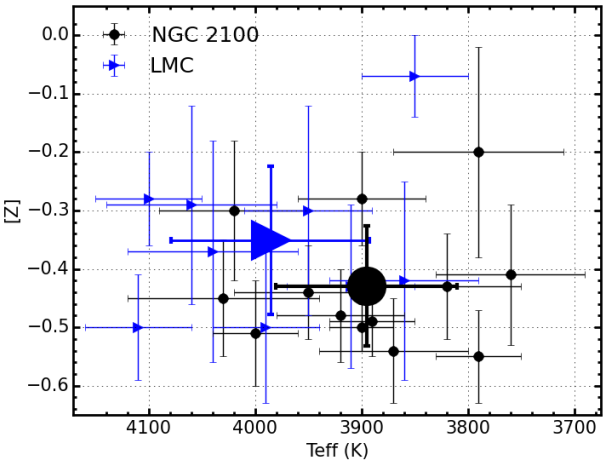

Figure 6. Estimated metallicities for NGC 2100 RSGs in this study shown against effective temperature (black points). For comparison we show the distribution of LMC RSGs from Davies et al. (2015, blue triangles) with good agreement between the means of the two samples.

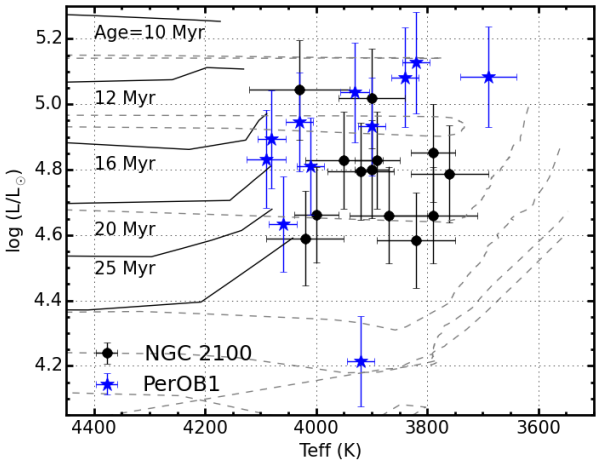

Figure 7. H–R diagram for 14 RSGs in NGC 2100 (black points). Isochrones for solar (dashed grey lines; Ekström et al. 2012) and SMC-like (solid black lines; Georgy et al. 2013) metal abundances, in which stellar rotation is 40% of the break-up velocity, are shown for ages of 10-32 Myr. For comparison, 11 RSGs from the Galactic YMC Perseus OB-1 are overlaid with blue stars (Gazak et al. 2014a). The best-fit isochrone to the observed data has an age of 20 ± 5 Myr for both SMC- and solar-like metallicities.

Table 3. Model grid used for the spectroscopic analysis.

Model Parameter	Min.	Max.	Step size
$T_{\rm eff}$ (K)	3400	4400	100
[Z] (dex)	−1.0	1.0	0.1
$\log g$ (cgs)	−1.00	1.00	0.25
ξ (km s^{-1})	1.0	5.0	0.2

sonable agreement with our estimate. There are three targets in common with our study: B17, C2 and C32 (using the Robertson 1974, nomenclature). Given the differences in the analyses (i.e. optical cf. infrared, and the different models used) the estimated parameters are in reasonable agreement for all three stars (aside from the spectroscopic gravities quoted by JT94, but with reasonable agreement with their photometric gravity estimates).

Using the same analysis technique as in this study, Davies et al. (2015) estimate metallicities for nine RSGs within the LMC, finding an average value of [Z] $= -0.37 \pm 0.14$ dex, which our estimate agrees well with. In Figure 6, we compare the effective temperatures and metallicities from NGC 2100 with those estimated for RSGs elsewhere in the LMC. We find good agreement in the distribution of temperatures from the two studies, with the average agreeing well. The range in [Z] from the LMC population is slightly larger than that of the NGC 2100 RSGs, which is expected when comparing a star cluster with an entire galaxy; however, the averages for the two studies agree very well.

4 DISCUSSION

4.1 Stellar parameters

Luminosities have been estimated for our sample from *K*-band photometry (see Table 1) using the bolometric correction from Davies, B., et al. (2013) with a small contribution from interstellar extinction using E(B−V) = 0.17 (Niederhofer et al. 2015) assuming $R_V = 3.5$ (Doran et al. 2013) and $A_K/A_V = 0.112$ (Rieke & Lebofsky 1985). The H–R diagram for the cluster is presented in Figure 7. Overlaid on this H–R diagram are SYCLIST stellar isochrones for SMC-like (solid lines; Georgy et al. 2013) and Solar-like (dashed lines; Ekström et al. 2012) models, where stellar rotation is 40% of break-up velocity. Even though the temperatures covered by the SMC-like models do not represent the distribution of temperatures observed in this study, they remain useful to constrain the age of NGC 2100. The Solar-like models (dashed) demonstrate that, when compared with the SMC-like models, increasing the metallicity of the sample (a) decreases the average temperature of the RSGs (something which is not observed by Patrick et al. 2015), (b) induces so-called 'blue loop' behaviour for the youngest models and (c) decreases the luminosity for the youngest models. The best-fitting model to the observed data has an age of 20 ± 5 Myr, in reasonable agreement with the estimate in Beasor & Davies (submitted).

In addition, results for 11 RSGs from the Galactic star cluster Perseus OB-1 (PerOB1; Gazak et al. 2014b) are overlaid in Figure 7 (blue stars) for which stellar parameters were estimated using the same analysis technique as in this study. PerOB1 is a cluster with a similar mass and age (2×10^4 M$_\odot$ and 14 Myr respectively; Currie et al. 2010) as NGC 2100, and a comparison between the stellar components of these two clusters using a consistent analysis technique is useful to highlight differences in stellar evolution within clusters at this range of metallicities.

We can see from Figure 7 that, generally, the estimated temperatures are in good agreement between the two clusters. The median luminosity for the PerOB1 targets ($10^{4.93 \pm 0.15}$ L$_\odot$) is slightly above that of NGC 2100

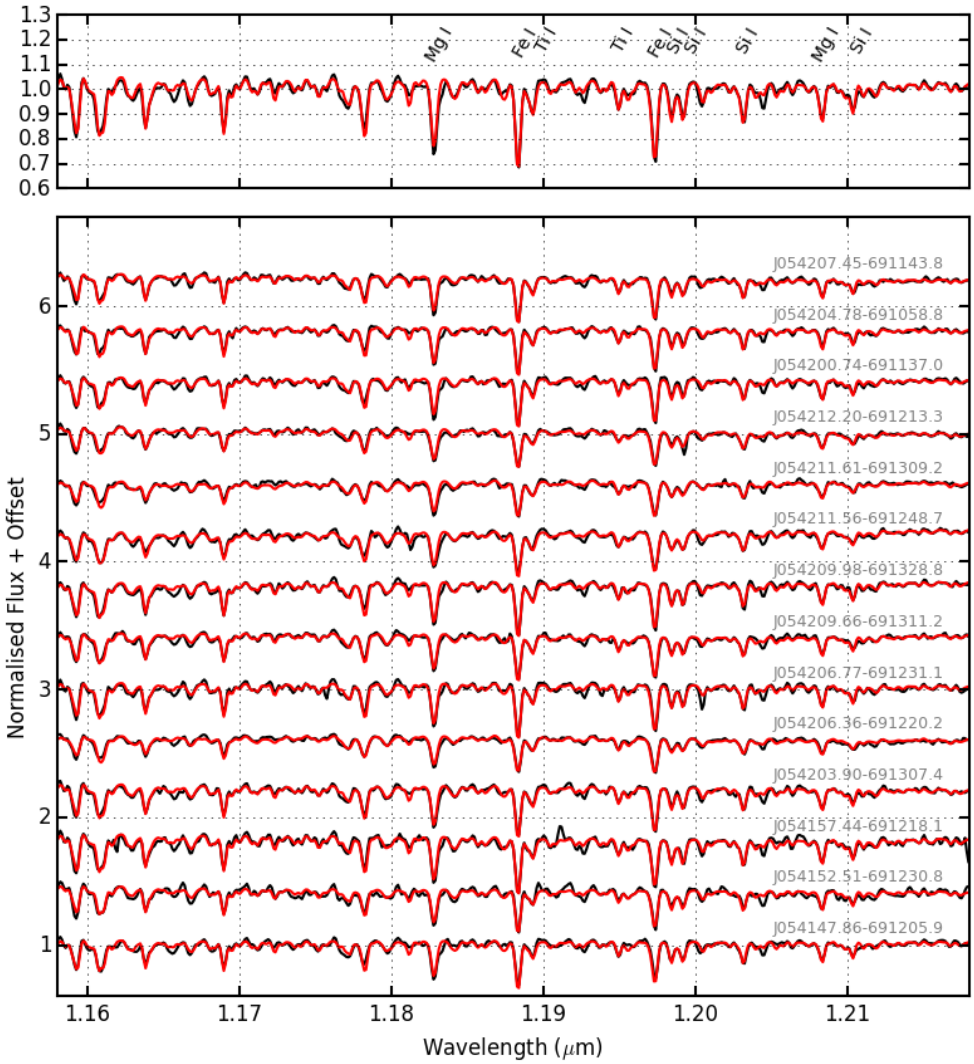

Figure 5. KMOS spectra of RSGs in NGC 2100 and their associated best-fit models (black and red lines, respectively). The upper panel shows the simulated integrated-light cluster spectrum; the lower panel shows spectra for the individual RSGs. The lines used for the analysis, from left-to-right by species, are Fe I λλ1.188285, 1.197305; Mg I λλ1.182819, 1.208335; Si I λλ1.198419, 1.199157, 1.203151, 1.210353; Ti I λλ1.189289, 1.194954.

($10^{4.77\pm0.15}\,L_{\odot}$) which could represent the slight difference in the ages of the two clusters. As PerOB1 is younger, the average mass for a RSG in the cluster will be larger than the average in NGC 2100. Therefore, we would expect to see higher luminosity RSGs in PerOB1. However, the difference between the two samples is barely significant and is consistent with a constant luminosity. The average effective temperatures for the two data sets (NGC 2100: 3890 ± 20 K, PerOB1: 3940 ± 10 K) are in reasonable agreement, where the spread in temperatures is slightly larger for PerOB1 ($\sigma_{\rm PerOB1} = 120$ K, $\sigma_{\rm NGC\,2100} = 85$ K), particularly so for the highest luminosity targets within the PerOB1 sample. Overall, by comparing these two star clusters with a similar mass, age and stellar population, we conclude that there exists no significant difference in appearance on the H–R diagram of RSGs within these star clusters of different metallicities.

The stellar parameters have been estimated assuming a Solar-like [α/Fe] = 0.0. As we have recently included the non-LTE corrections for two strong Mg I lines (Bergemann et al. 2015) we now have the tools to estimate the [α/Fe] given that we have increased the number of diagnostic lines used as well as the number of α elements. We do not include [α/Fe] as a free parameter in our model as the [α/Fe] for the LMC appears to be within ± 0.2 (see Davies et al. 2015, and references therein). In the near future we will introduce the [α/Fe] as a free parameter in this analysis routine where its dependencies and any potential degeneracies will be quantified rigorously, however, this is beyond the scope of the present study.

4.2 Simulated cluster spectrum analysis

We can use the individual stars in NGC 2100 to simulate the analysis of a YMC in the more distant Universe, using the assumption that RSGs dominate the near-IR flux from such a cluster (Gazak et al. 2013). Gazak et al. (2014a) use

Table 4. Physical parameters determined for the KMOS targets in NGC 2100.

Target	IFU	ξ (km s^{-1})	[Z]	log g	$T_{\rm eff}$ (K)	Notes[a]
J054147.86−691205.9	7	3.6 ± 0.2	-0.45 ± 0.10	0.10 ± 0.16	4030 ± 90	D15
J054152.51−691230.8	9	3.6 ± 0.2	-0.51 ± 0.09	0.43 ± 0.18	4000 ± 40	D16
J054157.44−691218.1	6	4.9 ± 0.1	-0.44 ± 0.08	0.15 ± 0.20	3950 ± 70	C2
J054200.74−691137.0	4	4.2 ± 0.2	-0.55 ± 0.08	0.23 ± 0.10	3790 ± 40	C8
J054203.90−691307.4	12	4.5 ± 0.2	-0.49 ± 0.06	0.23 ± 0.09	3890 ± 40	B4
J054204.78−691058.8	3	4.2 ± 0.2	-0.54 ± 0.09	0.46 ± 0.15	3870 ± 70	...
J054206.36−691220.2	24	2.8 ± 0.4	-0.20 ± 0.18	0.42 ± 0.18	3790 ± 80	B17
J054206.77−691231.1	10	4.9 ± 0.2	-0.50 ± 0.04	0.25 ± 0.09	3900 ± 30	A127
J054207.45−691143.8	2	4.0 ± 0.2	-0.43 ± 0.09	0.45 ± 0.17	3820 ± 70	C12
J054209.66−691311.2	14	3.8 ± 0.2	-0.41 ± 0.12	0.06 ± 0.20	3760 ± 70	B47
J054209.98−691328.8	11	4.8 ± 0.1	-0.48 ± 0.08	0.17 ± 0.22	3920 ± 60	C32
J054211.56−691248.7	20	3.8 ± 0.2	-0.28 ± 0.08	0.01 ± 0.16	3900 ± 60	B40
J054211.61−691309.2	18	2.2 ± 0.4	0.23 ± 0.23	0.65 ± 0.19	3800 ± 100	B46
J054212.20−691213.3	22	3.3 ± 0.2	-0.30 ± 0.12	0.33 ± 0.31	4020 ± 70	B22
NGC 2100 average[b]		4.0 ± 0.6	-0.43 ± 0.10	0.25 ± 0.15	3890 ± 85	
Integrated-light spectrum[c]		4.6 ± 0.3	-0.42 ± 0.14	0.37 ± 0.22	3860 ± 85	

[a] ID in final column from Robertson (1974).
[b] Averages computed excluding J054211.61−691309.2. See text for details.
[c] Simulated integrated light cluster spectrum parameters estimated excluding J054211.61−691309.2.

this assumption to create a simulated integrated-light cluster spectrum for PerOB1 and show that, by analysing the combined spectrum from their 11 RSGs, the resulting parameters are consistent with the average parameters estimated using the individual stars. NGC 2100 has a similar mass and age to PerOB1 and Gazak et al. (2014a) study a similar number of RSGs to this study, therefore, a direct comparison between the two clusters is useful to investigate potential metallicity dependencies.

To create a simulated integrated-light cluster spectrum we sum all the individual RSG spectra weighted by their J-band luminosities. The resulting spectrum is then degraded to the lowest resolution spectrum of the sample using a simple Gaussian filter. The top panel of Figure 5 shows the resulting integrated-light cluster spectrum. This spectrum is then analysed in the same way described in Section 3.3 for a single RSG. The results of this analysis are what one would expect from KMOS observations of more distant YMCs where individual stars cannot be resolved. We find a metallicity of -0.42 ± 0.14 dex, an effective temperature of 3860 ± 85 K, a surface gravity of 0.37 ± 0.22 dex and a microturbulent velocity of 4.6 ± 0.3 km s^{-1} which agree well with the averages of the individual RSG parameters.

4.3 Velocity dispersion and dynamical mass

This study represents the first estimate of an upper limit to the line-of-sight velocity dispersion profile for NGC 2100. Comparing this estimate with that of other YMCs in the Local Universe is useful to ascertain if this cluster shares similar properties with other YMCs. We find the properties NGC 2100 are well matched by other clusters with similar masses and ages, particularly so with RSGC01, a Galactic YMC (Davies et al. 2007).

Owing to the non-negligible contribution from measurement errors, the σ_{1D} adopted here is an upper limit to the true dispersion within the cluster which is likely to be significantly smaller. Using the data available, we can rule out an σ_{1D} value significantly larger than 3.9 km s^{-1}, however, the true dispersion of the cluster is unresolved.

By extension, the dynamical mass estimated here is therefore also an upper limit to the true mass of the cluster. There are several factors that could alter the value of the dynamical mass estimate. The likely value of the η parameter is discussed in Section 3.2 and any change in this value will act to decrease the estimated dynamical mass.

5 CONCLUSIONS

Using KMOS spectra of 14 RSGs in NGC 2100 we have estimated the dynamical properties of this YMC for the first time. Radial velocities have been estimated to a precision of < 5 km s^{-1}demonstrating that KMOS can be used to study the dynamical properties of star clusters in external galaxies.

An upper limit to the average line-of-sight velocity dispersion of $\sigma_{1D} = 3.9$ km s^{-1} has been estimated, at the 95% confidence level, and we find no evidence for spatial variations. Using the average velocity dispersion within NGC 2100 allows an upper limit on the dynamical mass to be calculated (assuming virial equilibrium) as $M_{dyn} = 15.2 \times 10^4 M_{\odot}$. This measurement is consistent with the literature measurement of the photometric mass (McLaughlin & van der Marel 2005) as the true dispersion is unresolved.

In addition to estimating the dynamical properties of NGC 2100, we have also estimated stellar parameters for the RSGs in NGC 2100 using the new J-band analysis technique (Davies et al. 2010). We find the average metallicity for RSGs in NGC 2100 is [Z] $= -0.43 \pm 0.10$ dex, which agrees well with previous studies within this cluster and with studies of the young stellar population of the LMC.

The H–R diagram of NGC 2100 is compared with that of PerOB1: a Galactic YMC with a similar age, mass and stellar population. Using stellar parameters estimated from Gazak et al. (2014a), obtained with the same technique as in this study, we demonstrate that there is no significant difference in the appearance of the H–R diagram of YMCs between Solar- and LMC-like metallicities.

By combining the individual RSG spectra within

NGC 2100, we have simulated an integrated-light cluster spectrum and proceeded to analyse this spectrum using the same techniques for that of the individual RSGs, as RSGs dominate the cluster light in the J-band (Gazak et al. 2013). The results of this technique demonstrate the potential of this analysis for integrated light spectra of more distant YMCs in low-metallicity environments. We find good agreement using the integrated-light cluster spectrum with the average results of the individual RSGs.

ACKNOWLEDGEMENTS

The authors would like to thank the anonymous referee for a careful review which has improved the quality of this publication. In addition, we would like to thank A. Hall for discussions surrounding Bayesian probabilities, M. Gieles and A.-L. Varri for helpful discussions and suggestions. Based on observations collected at the European Organisation for Astronomical Research in the Southern Hemisphere under ESO programme 095.B-0022(A).

REFERENCES

Bergemann, M., Kudritzki, R.-P., Plez, B., et al. 2012, ApJ, 751, 156
Bergemann, M., Kudritzki, R.-P., Würl, M., et al. 2013, ApJ, 764, 115
Bergemann, M., Kudritzki, R.-P., Gazak, Z., Davies, B., & Plez, B. 2015, ApJ, 804, 113
Cabrera-Ziri, I., Bastian, N., Davies, B., et al. 2014, MNRAS, 441, 2754
Cioni, M.-R. L., Clementini, G., Girardi, L., et al. 2011, A&A, 527, A116
Crowther, P. A., Schnurr, O., Hirschi, R., et al. 2010, MNRAS, 408, 731
Currie, T., Hernandez, J., Irwin, J., et al. 2010, ApJS, 186, 191
Davies, B., Figer, D. F., Kudritzki, R.-P., et al. 2007, ApJ, 671, 781
Davies, B., Origlia, L., Kudritzki, R.-P., et al. 2009, ApJ, 696, 2014
Davies, B., Kudritzki, R.-P., & Figer, D. F. 2010, MNRAS, 407, 1203
Davies, B., Kudritzki, R.-P., Plez, B., et al. 2013, ApJ, 767, 3
Davies, B., Kudritzki, R.-P., Gazak, Z., et al. 2015, ApJ, 806, 21
Davies, R. I., Agudo Berbel, A., Wiezorrek, E., et al. 2013, A&A, 558, A56
de Grijs, R., Wicker, J. E., & Bono, G. 2014, AJ, 147, 122
de Wit, W. J., Testi, L., Palla, F., & Zinnecker, H. 2005, A&A, 437, 247
Doran, E. I., Crowther, P. A., de Koter, A., et al. 2013, A&A, 558, A134
Ekström, S., Georgy, C., Eggenberger, P., et al. 2012, A&A, 537, A146
Eldridge, J. J., Izzard, R. G., & Tout, C. A. 2008, MNRAS, 384, 1109
Elson, R. A. W. 1991, ApJS, 76, 185
Evans, C. J., Davies, B., Kudritzki, R.-P., et al. 2011, A&A, 527, A50
Evans, C. J., van Loon, J. T., Hainich, R., & Bailey, M. 2015, A&A, 584, A5
Feast, M. W. 1979, MNRAS, 186, 831
Foreman-Mackey, D., Hogg, D. W., Lang, D., & Goodman, J. 2013, PASP, 125, 306
Gazak, J. Z., Bastian, N., Kudritzki, R.-P., et al. 2013, MNRAS, 430, L35
Gazak, J. Z., Davies, B., Kudritzki, R., Bergemann, M., & Plez, B. 2014a, ApJ, 788, 58
Gazak, J. Z., Davies, B., Bastian, N., et al. 2014b, ApJ, 787, 142
Gazak, J. Z., Kudritzki, R., Evans, C., et al. 2015, ApJ, 805, 182
Georgy, C., Ekström, S., Eggenberger, P., et al. 2013, A&A, 558, A103
Gieles, M., Sana, H., & Portegies Zwart, S. F. 2010, MNRAS, 402, 1750
Goodman, J., & Weare, J. 2010, Comm. App. Math. Comp. Sci., 5(1), 65
Gratton, R. G., Carretta, E., & Bragaglia, A. 2012, A&A Rev., 20, 50
Gustafsson, B., Edvardsson, B., Eriksson, K., et al. 2008, A&A, 486, 951
Hénault-Brunet, V., Evans, C. J., Sana, H., et al. 2012, A&A, 546, A73
Jasniewicz, G., & Thevenin, F. 1994, A&A, 282, 717
King, I. R. 1966, AJ, 71, 64
Lada, C. J., & Lada, E. A. 2003, ARA&A, 41, 57
Lapenna, E., Origlia, L., Mucciarelli, A., et al. 2015, ApJ, 798, 23
Lardo, C., Davies, B., Kudritzki, R.-P., et al. 2015, ApJ, 812, 160
Mackey, A. D., & Gilmore, G. F. 2003, MNRAS, 338, 85
Massey, P., & Hunter, D. A. 1998, ApJ, 493, 180
McLaughlin, D. E., & van der Marel, R. P. 2005, ApJS, 161, 304
Miller, B. W., Whitmore, B. C., Schweizer, F., & Fall, S. M. 1997, AJ, 114, 2381
Niederhofer, F., Hilker, M., Bastian, N., & Silva-Villa, E. 2015, A&A, 575, A62
Parker, R. J., & Goodwin, S. P. 2007, MNRAS, 380, 1271
Patrick, L. R., Evans, C. J., Davies, B., et al. 2015, ApJ, 803, 14
Pietrzyński, G., Graczyk, D., Gieren, W., et al. 2013, Nature, 495, 76
Points, S. D., Chu, Y. H., Kim, S., et al. 1999, ApJ, 518, 298
Portegies Zwart, S. F., McMillan, S. L. W., & Gieles, M. 2010, ARA&A, 48, 431
Rieke, G. H., & Lebofsky, M. J. 1985, ApJ, 288, 618
Robertson, J. W. 1974, A&AS, 15, 261
Sharples, R., Bender, R., Agudo Berbel, A., et al. 2013, The Messenger, 151, 21
Whitmore, B. C., & Schweizer, F. 1995, AJ, 109, 960
Zepf, S. E., Ashman, K. M., English, J., Freeman, K. C., & Sharples, R. M. 1999, AJ, 118, 752